Järvenpää, Seppo; Wallén, Henrik

Faster Conversion between Multipole Series and Plane Waves for Broadband MLFMA

Published in:
IEEE Transactions on Antennas and Propagation

DOI:
10.1109/TAP.2019.2905722

Published: 01/06/2019

Document Version
Peer reviewed version

Please cite the original version:
Järvenpää, S., & Wallén, H. (2019). Faster Conversion between Multipole Series and Plane Waves for Broadband MLFMA. *IEEE Transactions on Antennas and Propagation*, *67*(6), 3987-3995. [8668451]. https://doi.org/10.1109/TAP.2019.2905722

Faster Conversion between Multipole Series and Plane Waves for Broadband MLFMA

Seppo Järvenpää and Henrik Wallén

***Abstract*—A new efficient approach for converting multipole series coefficients to plane wave samples and back is presented in detail. The presented algorithm utilizes the fast Fourier transform in order to speed up the process. It can be used to develop an efficient implementation of a broadband multilevel fast multipole algorithm (MLFMA). The numerical tests demonstrate that the presented process also allows full numerical error control, which is an important factor in a practical implementation.**

***Index Terms*—Multilevel fast multipole algorithm; Method of moments; Fast Fourier transform; Interpolation; Anterpolation;**

I. Introduction

MULTILEVEL fast multipole algorithm (MLFMA) [1]–[4] can be used to expedite system matrix-vector products while solving systems of equations arising from integral equations. The standard high frequency version utilizes Rokhlin's translator, which is known to suffer from a *low frequency breakdown* [5], and therefore alternative methods for processing sub-wavelength levels must be considered.

A relatively simple solution is to combine the high frequency MLFMA with a process that utilizes multipole series for sub-wavelength levels. However, the translations with multipole series are laborious since the translator is not *diagonal*.

An alternative solution is to employ a spectral translator [6], [7] and similar plane wave samples as in the high frequency part. The problem in this particular approach is that although the translator is diagonal, one must now aggregate and disaggregate *six* sample patterns, one for each positive and negative main direction. This consumes resources and significantly slows down the algorithm.

In this paper the following strategy is considered: We combine a spectral translator with the improved version of *trigonometric polynomial expansion based* MLFMA (referred here as TPE-MLFMA) [8], [9], [10]. The propagating part is first aggregated, translated and disaggregated with the standard TPE interpolators. As it will be demonstrated in this paper, the required characteristic function fits nicely into this scheme and does not cause any numerical problems for these type of interpolators. Then the evanescent part is taken care of with a completely separate process. Aggregation and disaggregation for the evanescent part is performed with multipole series, and the multipole series coefficients are converted into plane wave samples for the application of the spectral translator, and then afterwards converted back into incoming multipole series coefficients. The question of how this conversion takes place plays a crucial role, especially since it requires a lot of CPU resources, and therefore a careful design of the algorithms is a very important factor. This paper borrows heavily on the ideas presented in [11], [12], and then improves them in order to obtain a significant speedup for this particular process.

The outline of the article is as follows. In Section II spectral translator is introduced, and in the following section a simple way to compute the propagating part of the translation is presented. In Section IV numerical evaluation of the evanescent contribution coming from the spectral translator is shortly discussed, and then in Sections V and VI the actual fast algorithms for the conversion forward and back are given, respectively. The paper ends with an investigation of the speedup and accuracy of the presented algorithms (Section VII) and conclusions (Section VIII).

The authors are with the Department of Electronics and Nanoengineering, Aalto University, P.O. Box 15500, FI-00076 Aalto, Finland (email: henrik.wallen@aalto.fi)

II. Spectral translator

Let us consider calculation of

$$F(\mathbf{D}+\mathbf{r}) = \int_{Q_1} G(\mathbf{D}+\mathbf{r}-\mathbf{r}')\rho(\mathbf{r}')\,d\mathbf{r}', \tag{1}$$

where Q_1 is the source cube on level $\ell \in \mathbb{Z}$ with side length $d_\ell = 2^{\ell-1}\lambda = 2^\ell \pi/k$, ρ the source distribution,

$$\mathbf{D} = [D_1, D_2, D_3]^T = d_\ell[\tilde{d}_1, \tilde{d}_2, \tilde{d}_3]^T,\ \tilde{d}_i \in \mathbb{Z} \tag{2}$$

is the vector from the center point of Q_1 to the center point of the target cube Q_2 (where $\mathbf{r}$ is located, see Fig. 1) and the Green's function is

$$G(\mathbf{r}) = \frac{e^{ik|\mathbf{r}|}}{4\pi|\mathbf{r}|}. \tag{3}$$

The integral in Eq. (1) can be calculated with a representation

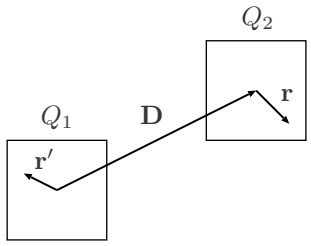

Fig. 1. The setup for Eq. (1).

of the form

$$F(\mathbf{D}+\mathbf{r}) = \int_{Q_1} \left(\int_S T(\mathbf{D},\hat{\mathbf{k}})\, e^{ik\hat{\mathbf{k}}\cdot(\mathbf{r}-\mathbf{r}')}\, d\hat{\mathbf{k}} \right) \rho(\mathbf{r}')\, d\mathbf{r}'$$

$$= \int_S T(\mathbf{D},\hat{\mathbf{k}})\, F^\infty(\hat{\mathbf{k}})\, e^{ik\hat{\mathbf{k}}\cdot\mathbf{r}}\, d\hat{\mathbf{k}} = \int_S V(\hat{\mathbf{k}})\, e^{ik\hat{\mathbf{k}}\cdot\mathbf{r}}\, d\hat{\mathbf{k}}, \quad (4)$$

where S is the surface of the unit sphere, i.e.

$$\hat{\mathbf{k}}(\theta,\varphi) = \cos\varphi\, \sin\theta\, \hat{\mathbf{e}}_1 + \sin\varphi\, \sin\theta\, \hat{\mathbf{e}}_2 + \cos\theta\, \hat{\mathbf{e}}_3, \quad (5)$$

and

$$S = \{\, \hat{\mathbf{k}}(\theta,\varphi) \mid 0 \le \theta \le \pi,\, 0 \le \varphi < 2\pi \,\}. \quad (6)$$

In suitably high levels, for example $\ell \ge 1$, one can utilize the Rokhlin translation function [1] as function T in (4). By inspecting Eq. (4) one can observe that the *outgoing far field pattern* F^∞ has been defined here as follows

$$F^\infty(\hat{\mathbf{k}}) = \int_{Q_1} e^{-ik\hat{\mathbf{k}}\cdot\mathbf{r}'} \rho(\mathbf{r}')\, d\mathbf{r}', \quad (7)$$

and the *incoming field pattern* is

$$V(\hat{\mathbf{k}}) = T(\mathbf{D},\hat{\mathbf{k}})\, F^\infty(\hat{\mathbf{k}}), \quad \hat{\mathbf{k}} \in S. \quad (8)$$

On levels consisting of cubes with sub-wavelength size, i.e. $\ell \le 0$, one can for example utilize *spectral translator* [6], [7], and the integration domain, in the case of $\hat{\mathbf{e}}_3 \cdot (\mathbf{D}+\mathbf{r}) > 0$, is

$$C_{\mathtt{pro/eva}} = \{\hat{\mathbf{k}}(\theta,\varphi) \,|\, \theta \in \Gamma_{\mathtt{pro/eva}},\ 0 \le \varphi < 2\pi\}, \quad (9)$$

where

$$\Gamma_{\mathtt{pro}} = \{\, \theta \,|\, 0 \le \theta \le \pi/2\}, \quad (10)$$

$$\Gamma_{\mathtt{eva}} = \{\, \theta \,|\, \theta = \pi/2 - it,\, t > 0\}, \quad (11)$$

and the actual translator [6] is

$$T(\mathbf{D},\hat{\mathbf{k}}) = \frac{ik}{8\pi^2} e^{ik\hat{\mathbf{k}}\cdot\mathbf{D}}. \quad (12)$$

In this case, as indicated in (9), Eq. (4) can be divided into so called *propagating* and *evanescent* parts

$$F(\mathbf{D}+\mathbf{r}) = F_{\mathtt{pro}}(\mathbf{D}+\mathbf{r}) + F_{\mathtt{eva}}(\mathbf{D}+\mathbf{r})$$

$$= \int_0^{2\pi}\int_0^{\pi/2} T(\mathbf{D},\hat{\mathbf{k}}(\theta,\varphi))\, F^\infty(\hat{\mathbf{k}}(\theta,\varphi))\, e^{ik\hat{\mathbf{k}}(\theta,\varphi)\cdot\mathbf{r}} \sin\theta\, d\varphi\, d\theta$$

$$-i\int_0^{2\pi}\int_0^{\infty} T(\mathbf{D},\hat{\mathbf{k}}(\theta(t),\varphi)) \times$$

$$F^\infty(\hat{\mathbf{k}}(\theta(t),\varphi))\, e^{ik\hat{\mathbf{k}}(\theta(t),\varphi)\cdot\mathbf{r}}\, \sin(\theta(t))\, d\varphi\, dt, \quad (13)$$

where

$$\theta(t) = \frac{\pi}{2} - it. \quad (14)$$

The other five main directions can be taken care of by rotating the underlying coordinate system. For this purpose two new parameters are introduced here to denote the available choices, namely $p = 1,2,3$, which corresponds to each main axis $\hat{\mathbf{e}}_p$, and $\hat{s} = \pm 1$, which in turn corresponds to the positive or negative direction, respectively. These parameters are chosen for each cube pair (Q_1, Q_2) according to the dominating direction, i.e. one should choose p and $\hat{s}$, see Eq. (2), so that

$$|\tilde{d}_p| = \max_{j\in\{1,2,3\}} |\tilde{d}_j| \text{ and } \hat{s} = \mathrm{sign}(\tilde{d}_p),$$

and now $\hat{s}\,\hat{\mathbf{e}}_p \cdot (\mathbf{D}+\mathbf{r}) > 0$ holds assuming that cubes Q_1 and Q_2 do not touch each other.

III. Computation of the propagating part

The method presented in [13] works with TPE variant of MLFMA [8], [9], [10], and only the actual construction of the translator needs to be addressed here. However, for completeness we will briefly discuss the method in more detailed form, and provide the formulas that are not presented in [13].

The general idea of this approach is to write the first term on the right hand side of Eq. (13) in the form

$$F_{\mathtt{pro}}(\mathbf{D}+\mathbf{r}) =$$

$$\int_0^{2\pi}\int_0^{2\pi} \frac{1}{2} T(\mathbf{D},\hat{\mathbf{k}}) F^\infty(\hat{\mathbf{k}})\, e^{ik\hat{\mathbf{k}}\cdot\mathbf{r}}\, \chi(\theta,\varphi) |\sin\theta|\, d\varphi\, d\theta, \quad (15)$$

where the appropriate *spherical*, i.e. 2π-periodic and fulfilling

$$\chi(\theta,\varphi) = \chi(2\pi-\theta,\varphi+\pi), \quad \theta \in]\pi, 2\pi], \quad (16)$$

characteristic function is depending on the main direction of the translation

$$\chi(\theta,\varphi) =$$

$$\begin{cases} \chi_{[0,\pi]}(\theta)\, \tilde{\chi}(\varphi) + \chi_{[\pi,2\pi]}(\theta)\, \chi_{[\frac{\pi}{2},\frac{3\pi}{2}]}(\varphi), & p\hat{s} = +1, \\ \chi_{[0,\pi]}(\theta)\, \chi_{[\frac{\pi}{2},\frac{3\pi}{2}]}(\varphi) + \chi_{[\pi,2\pi]}(\theta)\, \tilde{\chi}(\varphi), & p\hat{s} = -1, \\ \chi_{[0,\pi]}(\theta)\, \chi_{[0,\pi]}(\varphi) + \chi_{[\pi,2\pi]}(\theta)\, \chi_{[\pi,2\pi]}(\varphi), & p\hat{s} = +2, \\ \chi_{[0,\pi]}(\theta)\, \chi_{[\pi,2\pi]}(\varphi) + \chi_{[\pi,2\pi]}(\theta)\, \chi_{[0,\pi]}(\varphi), & p\hat{s} = -2, \\ \tilde{\chi}(\theta), & p\hat{s} = +3, \\ \chi_{[\frac{\pi}{2},\frac{3\pi}{2}]}(\theta), & p\hat{s} = -3, \end{cases}$$

where $\tilde{\chi}(\phi) = \chi_{[0,\frac{\pi}{2}]}(\phi) + \chi_{[\frac{3\pi}{2},2\pi]}(\phi)$. The definitions of these functions are presented in Appendix I along with the formulas for the coefficients of the required Fourier series.

The required sampling rates for the translator are

$$\tilde{M} = \mathrm{exporder}\,(k|\mathbf{D}|, \mathtt{acc}) \quad (17)$$

and

$$\tilde{N}_m = \mathrm{exporder}\left(k \sin\theta_m^{\tilde{M}} \sqrt{D_1^2 + D_2^2}, \mathtt{acc}\right), \quad (18)$$

where $m = 0,\ldots,\tilde{M}$, $\mathtt{acc}$ is the requested accuracy (i.e. the relative error should remain below $10^{-\mathtt{acc}}$), exporder the function presented in [9] and

$$\theta_m^{\tilde{M}} = \frac{2\pi}{2\tilde{M}+1} m, \quad m = 0,\ldots,\tilde{M}. \quad (19)$$

Now the translator can be built according to the diagram depicted in Fig. 2. It should be noted that order M is the one used in the sampling of outgoing/incoming field patterns in θ-direction as presented in [9],

$$\tilde{Q}_m = \mathrm{exporder}\left(k \sin\theta_m^{2M+\tilde{M}} \sqrt{D_1^2 + D_2^2}, \mathtt{acc}\right) +$$

$$2\ \mathrm{exporder}\left(k \sin\theta_m^{2M+\tilde{M}} \frac{d_\ell}{\sqrt{2}}, \mathtt{acc}\right), \quad (20)$$

for $m = 0,\ldots,2M+\tilde{M}$, and

$$P_m = 2\ \mathrm{exporder}\left(k \sin\theta_m^{2M} \frac{d_\ell}{\sqrt{2}}, \mathtt{acc}\right), \quad (21)$$

for $m = 0,\ldots,2M$.

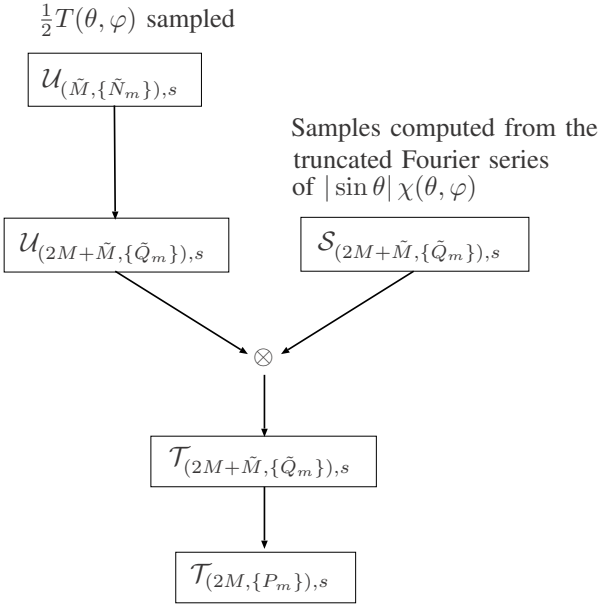

Fig. 2. Translator for the propagating part can be built according to this diagram. The Fourier series should be truncated to order $(2M+\tilde{M},\{\tilde{Q}_m\})$. If one utilizes the anterpolation version of [10], then the weights must also be incorporated to the translator at this stage.

To summarize, translation of the propagating part in low, i.e. sub-wavelength, levels in TPE-MLFMA requires only that in this particular case the now poorly functioning Rokhlin translator is replaced with the one shown in Eq. (12). However, efficient evaluation of the evanescent part in these levels is a more complicated operation. This will be considered in details in the next few sections.

IV. Computation of the evanescent part

Let us define $a_\ell = 2^\ell\pi = kd_\ell$. Change of variables [14]

$$\cos\theta = \frac{i}{a_\ell}s, \quad \sin\theta = \frac{1}{a_\ell}\sqrt{s^2+a_\ell^2} \tag{22}$$

results in

$$\hat{\mathbf{k}}(\theta,\varphi) = \frac{1}{a_\ell}\sqrt{s^2+a_\ell^2}\,(\cos\varphi\,\hat{\mathbf{e}}_1 + \sin\varphi\,\hat{\mathbf{e}}_2) + \frac{i}{a_\ell}s\,\hat{\mathbf{e}}_3, \tag{23}$$

and

$$F_{\mathtt{eva}}(\mathbf{D}+\mathbf{r}) = -\frac{i}{a_\ell}\int_0^{2\pi}\int_0^{\infty} T(\mathbf{D},\hat{\mathbf{k}}(\theta,\varphi))\times$$

$$F^\infty(\hat{\mathbf{k}}(\theta,\varphi))\,e^{ik\hat{\mathbf{k}}(\theta,\varphi)\cdot\mathbf{r}}\,d\varphi\,ds. \tag{24}$$

The previous integral has the following property: If one assumes that wave number k and source distribution ρ in Eq. (7) are real valued, then integral (24) is also real valued, and this fact can be used to test the performance of the method described in Section III independently (i.e. without actually implementing the evaluation of the evanescent part) by simply investigating how accurately the *imaginary part* of Green's function is translated through the process presented in that particular section. This approach will be employed in the numerical tests in Section VII.

To evaluate integral (24) a suitable numerical integration scheme is required. In parameter φ we employ a trapezoidal rule with $2\tilde{N}+1$ sampling points. On the other hand, with respect to parameter s we utilize a generalized Gaussian rule derived from the algorithm created by Yarvin and Rokhlin [15]. The sampling points $s_{\tilde{m}}$ and weights $w_{\tilde{m}}$, $\tilde{m}=1,\ldots,\tilde{M}$, and also order $\tilde{N}$ for the φ-integral, are available at https://users.aalto.fi/kwallen/equad; see also [13]. It should be noted that the size of the out-to-in -translation region affects the chosen $\tilde{M}$ and $\tilde{N}$. The ones given by `equad` are for the standard translation region. Let us denote the sampling points with

$$\hat{\mathbf{k}}_{\tilde{m}\tilde{n}} = \hat{\mathbf{k}}(\theta_{\tilde{m}},\varphi_{\tilde{n}}^{\tilde{N}}) = \frac{1}{a_\ell}\sqrt{s_{\tilde{m}}^2+a_\ell^2}\times$$

$$\left(\cos\varphi_{\tilde{n}}^{\tilde{N}}\,\hat{\mathbf{e}}_1 + \sin\varphi_{\tilde{n}}^{\tilde{N}}\,\hat{\mathbf{e}}_2\right) + \frac{i}{a_\ell}s_{\tilde{m}}\,\hat{\mathbf{e}}_3, \tag{25}$$

where

$$\varphi_{\tilde{n}}^{\tilde{N}} = \frac{2\pi}{2\tilde{N}+1}\tilde{n}, \quad \tilde{n}=0,\ldots,2\tilde{N}. \tag{26}$$

Integral (24) can then be evaluated with

$$F_{\mathtt{eva}}(\mathbf{D}+\mathbf{r}) \approx \sum_{\tilde{m}=1}^{\tilde{M}}\tilde{w}_{\tilde{m}}\sum_{\tilde{n}=0}^{2\tilde{N}} V_{\mathtt{eva}}(\hat{\mathbf{k}}_{\tilde{m}\tilde{n}})\,e^{ik\hat{\mathbf{k}}_{\tilde{m}\tilde{n}}\cdot\mathbf{r}}, \tag{27}$$

where

$$\tilde{w}_{\tilde{m}} = \frac{2\pi w_{\tilde{m}}}{2\tilde{N}+1} \tag{28}$$

and

$$V_{\mathtt{eva}}(\hat{\mathbf{k}}_{\tilde{m}\tilde{n}}) = -\frac{i}{a_\ell}T(\mathbf{D},\hat{\mathbf{k}}_{\tilde{m}\tilde{n}})\,F^\infty(\hat{\mathbf{k}}_{\tilde{m}\tilde{n}}). \tag{29}$$

V. Fast evaluation of plane wave samples from multipole series coefficients

In this section efficient computation of plane wave samples from multipole series coefficients, see Eq. (44) below, is investigated. The method presented by Bogaert et al. in [11] is derived in a detailed way, and then from Eq. (55) onward the algorithm is extended to a new faster version, see diagram (62) at the end of the section.

Let us begin by defining multipoles

$$Z_{n,m}^h(k\mathbf{r}) = h_n^{(1)}(kr)\,Y_{n,m}(\hat{\mathbf{r}}) \tag{30}$$

and

$$Z_{n,m}^j(k\mathbf{r}) = j_n(kr)\,Y_{n,m}(\hat{\mathbf{r}}), \tag{31}$$

where $r=|\mathbf{r}|$, $\hat{\mathbf{r}}=\mathbf{r}/r$, $h_n^{(1)}$ is the spherical Hankel function of the first kind, j_n is the spherical Bessel function of the first kind and $Y_{n,m}$ the normalized spherical harmonic defined by

$$Y_{n,m}(\hat{\mathbf{r}}) = Y_{n,m}(\theta,\varphi) = c_{nm}\,e^{im\varphi}P_n^m(\cos\theta) \tag{32}$$

where $0\le m\le n$,

$$\hat{\mathbf{r}} = \cos\varphi\sin\theta\,\hat{\mathbf{e}}_1 + \sin\varphi\sin\theta\,\hat{\mathbf{e}}_2 + \cos\theta\,\hat{\mathbf{e}}_3 \tag{33}$$

and

$$c_{nm} = \sqrt{\frac{2n+1}{4\pi}\frac{(n-m)!}{(n+m)!}}. \tag{34}$$

For negative indices we set

$$Y_{n,-m}(\hat{\mathbf{r}}) = (-1)^m \, Y^*_{n,m}(\hat{\mathbf{r}}^*). \tag{35}$$

Function P_n^m in Eq. (32) is the associated Legendre polynomial, or Ferrers function, as defined in [16, Ch. 14]. It should be noted that for fast evaluation definition (32) is not efficient, but rather alternative recursive formulas should be utilized, see for example the appendix of [12].

Green's function can be written in terms of multipoles [17]

$$\begin{aligned} G(\mathbf{r}-\mathbf{r}') &= \frac{e^{ik|\mathbf{r}-\mathbf{r}'|}}{4\pi|\mathbf{r}-\mathbf{r}'|} \\ &= ik\sum_{n=0}^{\infty}\sum_{m=-n}^{n} h^{(1)}(kr)\, Y_{n,m}(\hat{\mathbf{r}})\, j_n(kr')\, Y^*_{n,m}(\hat{\mathbf{r}}') \\ &= ik\sum_{n=0}^{\infty}\sum_{m=-n}^{n} (-1)^m Z^h_{n,m}(k\mathbf{r}) Z^j_{n,-m}(k\,\mathbf{r}'),\ |\mathbf{r}| > |\mathbf{r}'|, \end{aligned} \tag{36}$$

where identity (35) was used. This representation can be written as an outgoing multipole series, with additional *normalization coefficient* [4], $t_{out}^{\ell} := 2^{\ell}\pi$, added to the formulas results in

$$G(\mathbf{r}-\mathbf{r}') = \sum_{n=0}^{\infty}\left(t_{out}^{\ell}\right)^n \sum_{m=-n}^{n} \hat{a}_{nm}\, Z^h_{n,m}(k\,\mathbf{r}), \quad |\mathbf{r}| > |\mathbf{r}'|, \tag{37}$$

where the normalized coefficients are

$$\hat{a}_{nm} = ik(-1)^m \left(t_{out}^{\ell}\right)^{-n} Z^j_{n,-m}(k\,\mathbf{r}'). \tag{38}$$

The *normalized coefficients* $\hat{a}^{\infty}_{nm}$ for the corresponding the far field representation are then obtained with formula [17]

$$\hat{a}^{\infty}_{nm} = \frac{1}{k\, i^{n+1}}\, \hat{a}_{nm}, \tag{39}$$

i.e. one can then write in the case where the source in the cube consists of only one source point located at $\mathbf{r}'$,

$$F^{\infty}(\hat{\mathbf{k}}) = e^{-ik\hat{\mathbf{k}}\cdot\mathbf{r}'} = 4\pi\sum_{n=0}^{\infty}\left(t_{out}^{\ell}\right)^n \sum_{m=-n}^{n} \hat{a}^{\infty}_{nm}\, Y_{n,m}(\hat{\mathbf{k}}). \tag{40}$$

From Jacobi-Anger expansion [17]

$$e^{ik\mathbf{r}\cdot\hat{\mathbf{k}}} = \sum_{n=0}^{\infty} i^n (2n+1)\, j_n(kr)\, P_n(\hat{\mathbf{r}}\cdot\hat{\mathbf{k}}), \tag{41}$$

identity (35) and addition theorem [17]

$$\sum_{m=-n}^{n} Y_{n,m}(\hat{\mathbf{r}})\, Y^*_{n,m}(\hat{\mathbf{k}}^*) = \frac{2n+1}{4\pi} P_n(\hat{\mathbf{r}}\cdot\hat{\mathbf{k}}) \tag{42}$$

follows another useful expansion

$$e^{ik\hat{\mathbf{k}}\cdot\mathbf{r}} = 4\pi\sum_{n=0}^{\infty} i^n \sum_{m=-n}^{n} (-1)^m\, Y_{n,-m}(\hat{\mathbf{k}})\, Z^j_{n,m}(k\mathbf{r}), \tag{43}$$

which holds for any unit vector $\hat{\mathbf{k}}(\theta,\varphi) \in \mathbb{R}^3$. However, assuming that $\hat{\mathbf{k}}\cdot\hat{\mathbf{k}} = 1$, which is always the case for Eq. (5), Eq. (43) holds even with the complexified θ.

The samples of the outgoing far field pattern (40) can be computed from formula

$$F^{\infty}\left(\hat{\mathbf{k}}^{(p,\hat{s})}_{\tilde{m}\tilde{n}}\right) = 4\pi\sum_{n=0}^{N}\left(t_{out}^{\ell}\right)^n \sum_{m=-n}^{n} \hat{a}^{\infty}_{nm}\, Y_{n,m}\left(\hat{\mathbf{k}}^{(p,\hat{s})}_{\tilde{m}\tilde{n}}\right). \tag{44}$$

In this representation order N can be chosen as determined by function $\mathrm{evaorder}(\ell, \mathtt{acc})$ presented in [14].

In order to obtain formula for $\hat{\mathbf{k}}^{(p,\hat{s})}_{\tilde{m}\tilde{n}}$ used in the previous equation, let us investigate Eq. (12). One can write

$$\begin{aligned} T\left(\mathbf{D}, \hat{\mathbf{k}}^{(p,\hat{s})}_{\tilde{m}\tilde{n}}\right) &= \frac{ik}{8\pi^2} e^{ik\hat{\mathbf{k}}^{(p,\hat{s})}_{\tilde{m}\tilde{n}}\cdot\mathbf{D}} \\ &= \frac{ik}{8\pi^2} e^{ik\left(\hat{s}\mathbf{R}_p\hat{\mathbf{k}}^{(p,\hat{s})}_{\tilde{m}\tilde{n}}\cdot\hat{s}\mathbf{R}_p\mathbf{D}\right)}, \end{aligned} \tag{45}$$

where the rotation matrices are

$$\mathbf{R}_1 = \begin{bmatrix} 0 & 1 & 0 \\ 0 & 0 & 1 \\ 1 & 0 & 0 \end{bmatrix},\ \mathbf{R}_2 = \begin{bmatrix} 0 & 0 & 1 \\ 1 & 0 & 0 \\ 0 & 1 & 0 \end{bmatrix} \tag{46}$$

and

$$\mathbf{R}_3 = \begin{bmatrix} 1 & 0 & 0 \\ 0 & 1 & 0 \\ 0 & 0 & 1 \end{bmatrix}. \tag{47}$$

Now $\hat{\mathbf{e}}_3\cdot\hat{s}\,\mathbf{R}_p\mathbf{D} > 0$ holds, and one can utilize points $\hat{\mathbf{k}}_{\tilde{m}\tilde{n}}$, see (25), by simply defining $\hat{\mathbf{k}}^{(p,\hat{s})}_{\tilde{m}\tilde{n}}$ so that

$$\hat{\mathbf{k}}^{(p,\hat{s})}_{\tilde{m}\tilde{n}} := \hat{s}\,\mathbf{R}_p^{-1}\hat{\mathbf{k}}_{\tilde{m}\tilde{n}}. \tag{48}$$

By denoting the matrix that rotates a vector by angle α around axis $\hat{u}$ with $\mathbf{R}(\alpha,\hat{u})$, one can further write [11]

$$\hat{\mathbf{k}}^{(p,\hat{s})}_{\tilde{m}\tilde{n}} = \mathbf{R}_0^{-1}\left[\hat{s}\,\mathbf{R}\left(\frac{2p\pi}{3}, \hat{\mathbf{e}}_3\right)\right]\mathbf{R}_0\,\hat{\mathbf{k}}_{\tilde{m}\tilde{n}}, \tag{49}$$

where $\mathbf{R}_0 = \mathbf{R}\left(-\mathrm{acos}(1/\sqrt{3}), (\hat{\mathbf{e}}_2 - \hat{\mathbf{e}}_1)/\sqrt{2}\right)$.

Wigner rotation matrix $D^n \in \mathbb{R}^{(2n+1)\times(2n+1)}$ [18] is defined by formula

$$Y_{n,m}(\mathbf{R}\,\hat{\mathbf{r}}) = \sum_{m'=-n}^{n} D^n_{m,m'}(\mathbf{R})\, Y_{n,m'}(\hat{\mathbf{r}}), \tag{50}$$

where $\mathbf{R} \in \mathbb{R}^{3\times3}$ is a rotation matrix.

Eq. (44) can then be rewritten by utilizing the defined rotations and Wigner rotation matrix (50) as follows,

$$\begin{aligned} F^{\infty}\left(\hat{\mathbf{k}}^{(p,\hat{s})}_{\tilde{m}\tilde{n}}\right) &= 4\pi\sum_{n=0}^{N}\left(t_{out}^{\ell}\right)^n \sum_{m=-n}^{n} \hat{a}^{\infty}_{nm} \times \\ & Y_{n,m}\left(\mathbf{R}_0^{-1}\left[\hat{s}\,\mathbf{R}\left(\frac{2p\pi}{3}, \hat{\mathbf{e}}_3\right)\right]\mathbf{R}_0\,\hat{\mathbf{k}}_{\tilde{m}\tilde{n}}\right) \\ &= 4\pi\sum_{n=0}^{N}\sum_{m=-n}^{n} a'_{nm} Y_{n,m}\left(\hat{s}\,\mathbf{R}\left(\frac{2p\pi}{3}, \hat{\mathbf{e}}_3\right)\mathbf{R}_0\,\hat{\mathbf{k}}_{\tilde{m}\tilde{n}}\right), \end{aligned} \tag{51}$$

where

$$a'_{nm} = \left(t_{out}^{\ell}\right)^n \sum_{m'=-n}^{n} D^n_{m',m}(\mathbf{R}_0^{-1})\, \hat{a}^{\infty}_{nm'}. \tag{52}$$

Rotation around $\hat{\mathbf{e}}_3$ is diagonal, given by formula [11]

$$D^n_{m,m'}(\mathbf{R}(\alpha,\hat{\mathbf{e}}_3)) = e^{im\alpha}\delta_{m,m'}, \tag{53}$$

and so Eq. (51) can be written as

$$F^\infty\left(\hat{\mathbf{k}}^{(p,\hat{s})}_{\tilde{m}\tilde{n}}\right) =$$

$$4\pi\sum_{n=0}^{N}\hat{s}^n\sum_{m=-n}^{n}a'_{nm}e^{im\frac{2p\pi}{3}}Y_{n,m}(\mathbf{R}_0\,\hat{\mathbf{k}}_{\tilde{m}\tilde{n}}). \tag{54}$$

This formula was presented by Bogaert et al. in [11]. But one can observe now that representation (54) can be developed further into

$$F^\infty\left(\hat{\mathbf{k}}^{(p,\hat{s})}_{\tilde{m}\tilde{n}}\right) = 4\pi\sum_{n=0}^{N}\hat{s}^n\sum_{m=-n}^{n}c^{(p)}_{nm}\,Y_{n,m}(\hat{\mathbf{k}}_{\tilde{m}\tilde{n}})$$

$$= 4\pi\sum_{m=-N}^{N}\sum_{n=|m|}^{N}\hat{s}^n\,c^{(p)}_{nm}\,Y_{n,m}(\hat{\mathbf{k}}_{\tilde{m}\tilde{n}}), \tag{55}$$

where

$$c^{(p)}_{nm} = \sum_{m'=-n}^{n}D^n_{m',m}(\mathbf{R}_0)\,e^{im'\frac{2p\pi}{3}}\,a'_{nm'}$$

$$= \sum_{q=0}^{2}e^{iq\frac{2p\pi}{3}}\sum_{\substack{m'=-n\\ m' \bmod 3=q}}^{n}D^n_{m',m}(\mathbf{R}_0)\,a'_{nm'}. \tag{56}$$

According to Eq. (32) the far field pattern (55) has the form

$$F^\infty\left(\hat{\mathbf{k}}^{(p,\hat{s})}_{\tilde{m}\tilde{n}}\right) = \sum_{m=-N}^{N}b^{(p,\hat{s})}_{\tilde{m}}(m)\,e^{im\varphi^{\tilde{N}}_{\tilde{n}}}$$

$$= \sum_{m=-N}^{-\tilde{N}-1}b^{(p,\hat{s})}_{\tilde{m}}(m)\,e^{im\frac{2\pi}{2\tilde{N}+1}\tilde{n}}+$$

$$\sum_{m=-\tilde{N}}^{\tilde{N}}b^{(p,\hat{s})}_{\tilde{m}}(m)\,e^{im\frac{2\pi}{2\tilde{N}+1}\tilde{n}}+$$

$$\sum_{m=\tilde{N}+1}^{N}b^{(p,\hat{s})}_{\tilde{m}}(m)\,e^{im\frac{2\pi}{2\tilde{N}+1}\tilde{n}}, \tag{57}$$

where

$$b^{(p,\hat{s})}_{\tilde{m}}(m) =$$

$$\begin{cases} 0, & |m|>N,\\ 4\pi\displaystyle\sum_{n=|m|}^{N}c^{(p)}_{nm}\,\hat{s}^n\,Y_{n,m}(\hat{\mathbf{k}}_{\tilde{m}0}), & |m|\le N. \end{cases} \tag{58}$$

Since the chosen multipole series order N and the plane wave sampling rate in φ-direction $\tilde{N}$, see Eq. (26), are relatively close to each other, at least in the subwavelength levels, the major part of the computation typically takes place in the middle term of the right side of Eq. (57). The derived formulas can be used to speed up the computations simply because the middle term in question can be computed efficiently with `ifft`, see Appendix II, by first assembling vector

$$\mathbf{f}^{(p,\hat{s})}_{\tilde{m}} = [b^{(p,\hat{s})}_{\tilde{m}}(0),\ldots,b^{(p,\hat{s})}_{\tilde{m}}(\tilde{N}),$$
$$b^{(p,\hat{s})}_{\tilde{m}}(-\tilde{N}),\ldots,b^{(p,\hat{s})}_{\tilde{m}}(-1)], \tag{59}$$

and then computing for a given $\tilde{m}$

$$\mathbf{g}^{(p,\hat{s})}_{\tilde{m}} = (2\tilde{N}+1)\,\texttt{ifft}\left(\mathbf{f}^{(p,\hat{s})}_{\tilde{m}}\right). \tag{60}$$

Eq. (57) becomes then

$$F^\infty\left(\hat{\mathbf{k}}^{(p,\hat{s})}_{\tilde{m}\tilde{n}}\right) = \sum_{m=-N}^{-\tilde{N}-1}b^{(p,\hat{s})}_{\tilde{m}}(m)e^{im\frac{2\pi}{2\tilde{N}+1}\tilde{n}}+$$

$$\mathbf{g}^{(p,\hat{s})}_{\tilde{m}}(\tilde{n}) + \sum_{m=\tilde{N}+1}^{N}b^{(p,\hat{s})}_{\tilde{m}}(m)e^{im\frac{2\pi}{2\tilde{N}+1}\tilde{n}}. \tag{61}$$

So the computation of the plane wave samples starting with the outgoing normalized multipole series coefficients can be performed efficiently according to the following diagram:

$$\hat{a}^\infty \xrightarrow{(52)} a' \xrightarrow{(56)} \begin{Bmatrix} c^{(1)}\\ c^{(2)}\\ c^{(3)}\end{Bmatrix} \xrightarrow{(61)} \begin{Bmatrix} F^\infty(\hat{\mathbf{k}}^{(1,-1)})\\ F^\infty(\hat{\mathbf{k}}^{(1,+1)})\\ F^\infty(\hat{\mathbf{k}}^{(2,-1)})\\ F^\infty(\hat{\mathbf{k}}^{(2,+1)})\\ F^\infty(\hat{\mathbf{k}}^{(3,-1)})\\ F^\infty(\hat{\mathbf{k}}^{(3,+1)})\end{Bmatrix}. \tag{62}$$

VI. Fast evaluation of the coefficients of the incoming multipole series from the samples

After the translation operation each cube has six incoming sample pattern sets that must be converted into one incoming multipole series coefficient set. A new efficient version of this operation is derived in the section, see diagram (79) at the end of this section. To improve stability of the described process a suitable normalization coefficient t^ℓ_{in} is added to the formulas. From formulas (24), (29) and (43) it follows that

$$F_{\texttt{eva}}(\mathbf{D}+\mathbf{r}) = \sum_{p,\hat{s}}\int_0^{2\pi}\int_0^{\infty}V_{\texttt{eva}}\left(\hat{\mathbf{k}}^{(p,\hat{s})}\right)\,e^{ik\hat{\mathbf{k}}^{(p,\hat{s})}\cdot\mathbf{r}}\,d\varphi\,ds$$

$$= \sum_{p,\hat{s}}\int_0^{2\pi}\int_0^{\infty}V_{\texttt{eva}}\left(\hat{\mathbf{k}}^{(p,\hat{s})}\right)\times$$

$$\left[4\pi\sum_{n=0}^{\infty}i^n\sum_{m=-n}^{n}(-1)^mY_{n,-m}\left(\hat{\mathbf{k}}^{(p,\hat{s})}\right)\,Z^j_{n,m}(k\mathbf{r})\right]d\varphi\,ds$$

$$= \sum_{n=0}^{\infty}\left(t^\ell_{in}\right)^{-n}\sum_{m=-n}^{n}\hat{b}_{nm}\,Z^j_{n,m}(k\mathbf{r}), \tag{63}$$

where, see Eq. (35),

$$\hat{b}_{nm} = 4\pi i^n\left(t^\ell_{in}\right)^n\times$$

$$\sum_{p,\hat{s}}\int_0^{2\pi}\int_0^{\infty}V_{\texttt{eva}}\left(\hat{\mathbf{k}}^{(p,\hat{s})}\right)\,Y^*_{n,m}\left(\hat{\mathbf{k}}^{(p,\hat{s})*}\right)\,d\varphi\,ds. \tag{64}$$

Let us denote, following Eq. (39),

$$\hat{b}^{\infty}_{nm} = \frac{1}{k\, i^{n+1}}\, \hat{b}_{nm}. \tag{65}$$

Then the normalized coefficients for the incoming multipole series can be computed, see Eq. (49), with formula

$$\hat{b}^{\infty}_{nm} \simeq \frac{4\pi\, \left(t^{\ell}_{in}\right)^n}{ik} \sum_{\tilde{m},\tilde{n}} \tilde{w}_{\tilde{m}} \sum_{p,\hat{s}} V_{\mathtt{eva}}\left(\hat{\mathbf{k}}^{(p,\hat{s})}_{\tilde{m}\tilde{n}}\right) \times$$

$$Y^*_{n,m}\left(\mathbf{R}_0^{-1}\left[\hat{s}\,\mathbf{R}\left(\frac{2p\pi}{3},\hat{\mathbf{e}}_3\right)\right]\mathbf{R}_0\,\hat{\mathbf{k}}^*_{\tilde{m}\tilde{n}}\right), \tag{66}$$

where $\tilde{w}_{\tilde{m}}$ are the numerical integration quadrature weights defined in Section IV. To simplify notations let us further denote

$$\tilde{V}^{(p,\hat{s})}_{\tilde{m}\tilde{n}} := \tilde{w}_{\tilde{m}}\, V_{\mathtt{eva}}\left(\hat{\mathbf{k}}^{(p,\hat{s})}_{\tilde{m}\tilde{n}}\right). \tag{67}$$

Since the following identities

$$D^{n*}_{m_1,m_2}(\mathbf{R}) = D^{n}_{m_2,m_1}(\mathbf{R}^{-1}) \tag{68}$$

and

$$\sum_{m'=-n}^{n} D^{n}_{m',m_1}(\mathbf{R})\, D^{n*}_{m',m_2}(\mathbf{R}) = \delta_{m_1,m_2} \tag{69}$$

hold for any rotation matrix $\mathbf{R}$, coefficients $\hat{b}^{\infty}_{nm}$ can be written as

$$\hat{b}^{\infty}_{nm} = \sum_{m''=-n}^{n} \delta_{m,m''}\, \hat{b}^{\infty}_{nm''}$$

$$= \sum_{m''=-n}^{n}\left(\sum_{m'=-n}^{n} D^{n}_{m',m}(\mathbf{R}_0)\, D^{n*}_{m',m''}(\mathbf{R}_0)\right)\hat{b}^{\infty}_{nm''}$$

$$= \sum_{m''=-n}^{n}\left(\sum_{m'=-n}^{n} D^{n}_{m',m}(\mathbf{R}_0)\, D^{n}_{m'',m'}(\mathbf{R}_0^{-1})\right)\hat{b}^{\infty}_{nm''}$$

$$= \sum_{m'=-n}^{n} D^{n}_{m',m}(\mathbf{R}_0)\, \hat{b}'_{nm'}, \tag{70}$$

where

$$\hat{b}'_{nm'} = \sum_{m''=-n}^{n} D^{n}_{m'',m'}(\mathbf{R}_0^{-1})\, \hat{b}^{\infty}_{nm''}. \tag{71}$$

Combining this with (66) yields

$$b'_{nm} = \left(t^{\ell}_{in}\right)^{-n}\, \hat{b}'_{nm} = \frac{4\pi}{ik} \sum_{m''=-n}^{n} D^{n}_{m'',m}(\mathbf{R}_0^{-1}) \times$$

$$\sum_{\tilde{m},\tilde{n}}\sum_{p,\hat{s}} \tilde{V}^{(p,\hat{s})}_{\tilde{m}\tilde{n}}\, Y^*_{n,m''}\left(\mathbf{R}_0^{-1}\left[\hat{s}\,\mathbf{R}\left(\frac{2p\pi}{3},\hat{\mathbf{e}}_3\right)\right]\mathbf{R}_0\,\hat{\mathbf{k}}^*_{\tilde{m}\tilde{n}}\right)$$

$$= \frac{4\pi}{ik} \sum_{m''=-n}^{n} D^{n}_{m'',m}(\mathbf{R}_0^{-1}) \sum_{m'=-n}^{n} D^{n*}_{m'',m'}(\mathbf{R}_0^{-1}) \times$$

$$\sum_{\tilde{m},\tilde{n}}\sum_{p,\hat{s}} \tilde{V}^{(p,\hat{s})}_{\tilde{m}\tilde{n}}\, Y^*_{n,m'}\left(\left[\hat{s}\,\mathbf{R}\left(\frac{2p\pi}{3},\hat{\mathbf{e}}_3\right)\right]\mathbf{R}_0\,\hat{\mathbf{k}}^*_{\tilde{m}\tilde{n}}\right)$$

$$= \frac{4\pi}{ik} \sum_{\tilde{m},\tilde{n}}\sum_{p,\hat{s}} \tilde{V}^{(p,\hat{s})}_{\tilde{m}\tilde{n}}\, \hat{s}^n\, e^{-im\frac{2p\pi}{3}} Y^*_{n,m}\left(\mathbf{R}_0\,\hat{\mathbf{k}}^*_{\tilde{m}\tilde{n}}\right). \tag{72}$$

One can further simplify this into

$$b'_{nm} = \frac{4\pi}{ik} \sum_{p,\hat{s}} e^{-im\frac{2p\pi}{3}} \sum_{m'=-n}^{n} D^{n}_{m',m}(\mathbf{R}_0^{-1})\, \hat{s}^n \times$$

$$\sum_{\tilde{m},\tilde{n}} \tilde{V}^{(p,\hat{s})}_{\tilde{m}\tilde{n}}\, Y^*_{n,m'}\left(\hat{\mathbf{k}}^*_{\tilde{m}\tilde{n}}\right). \tag{73}$$

Let us then denote

$$d^{(p)}_{nm} := \frac{4\pi}{ik}(-1)^m \sum_{\tilde{m},\tilde{n}} Y_{n,-m}\left(\hat{\mathbf{k}}_{\tilde{m}\tilde{n}}\right) \sum_{\hat{s}} \hat{s}^n\, \tilde{V}^{(p,\hat{s})}_{\tilde{m}\tilde{n}}, \tag{74}$$

where Eq. (35) has been utilized, yielding

$$b'_{nm} = \sum_{m'=-n}^{n} D^{n}_{m',m}(\mathbf{R}_0^{-1}) \sum_{p=1}^{3} e^{-iq\frac{2p\pi}{3}}\, d^{(p)}_{nm'}, \tag{75}$$

where $q = m \bmod 3$. The required coefficients $d^{(p)}_{nm}$ can in turn be computed from formula

$$d^{(p)}_{nm} = \frac{4\pi}{ik}(-1)^m \sum_{\tilde{m}=1}^{\tilde{M}} \sum_{\tilde{n}=0}^{2\tilde{N}} e^{-im\frac{2\pi}{2\tilde{N}+1}\tilde{n}} \times$$

$$Y_{n,-m}\left(\hat{\mathbf{k}}_{\tilde{m}0}\right) \sum_{\hat{s}=\{-1,+1\}} \hat{s}^n\, \tilde{V}^{(p,\hat{s})}_{\tilde{m}\tilde{n}}. \tag{76}$$

For the case $-\tilde{N} \le m \le \tilde{N}$ the calculations can be made faster by first computing vectors, see Appendix II,

$$\mathbf{h}^{(p,\hat{s})}_{\tilde{m}} = \mathtt{fft}\left([\tilde{V}^{(p,\hat{s})}_{\tilde{m},0},\ldots,\tilde{V}^{(p,\hat{s})}_{\tilde{m},2\tilde{N}}]\right), \tag{77}$$

and then utilizing these to compute the coefficients for parameters $m = -\tilde{N},\ldots,\tilde{N}$ with

$$d^{(p)}_{nm} = \frac{4\pi}{ik}(-1)^m \sum_{\tilde{m}=1}^{\tilde{M}} Y_{n,-m}\left(\hat{\mathbf{k}}_{\tilde{m}0}\right) \sum_{\hat{s}=\{-1,+1\}} \hat{s}^n \times$$

$$\begin{cases} \mathbf{h}^{(p,\hat{s})}_{\tilde{m}}(2\tilde{N}+1+m), & -\tilde{N} \le m < 0, \\ \mathbf{h}^{(p,\hat{s})}_{\tilde{m}}(m), & 0 \le m \le \tilde{N}. \end{cases} \tag{78}$$

Thus the computation of incoming multipole series coefficients starting with the incoming plane wave samples can be performed with the following diagram:

$$\left\{\begin{array}{l} \tilde{V}(\hat{\mathbf{k}}^{(1,-1)}) \\ \tilde{V}(\hat{\mathbf{k}}^{(1,+1)}) \\ \tilde{V}(\hat{\mathbf{k}}^{(2,-1)}) \\ \tilde{V}(\hat{\mathbf{k}}^{(2,+1)}) \\ \tilde{V}(\hat{\mathbf{k}}^{(3,-1)}) \\ \tilde{V}(\hat{\mathbf{k}}^{(3,+1)}) \end{array}\right\} \xrightarrow[(78)]{(76)} \left\{\begin{array}{l} d^{(1)} \\ d^{(2)} \\ d^{(3)} \end{array}\right\} \xrightarrow{(75)} b' \xrightarrow{(70)} \hat{b}^{\infty}. \tag{79}$$

VII. Numerical results

The first test verifies that the process described in Section III works as anticipated. This was done by investigating the following test setup: First 6^3 source points were placed in a regular lattice from corner to corner inside each of the 8 small (side length $\lambda/8192$) cubes shown in Fig. 3. Each point i was also assigned with a random source $\rho_i \in \mathbb{R}$, see Eq. (1). The outgoing field patterns were then aggregated to

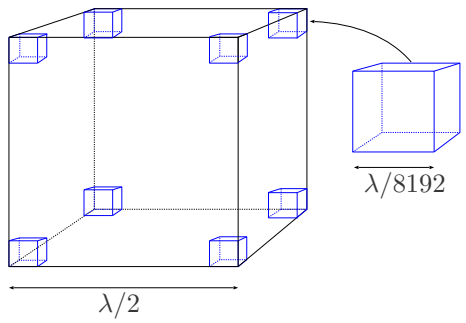

Fig. 3. Setup for the aggregation and disaggregation in the experiments. Notice that the eight small cubes (blue) are not in correct scale compared to the large one (black). To aggregate field from the small cubes to the large cube requires 12 interpolation steps.

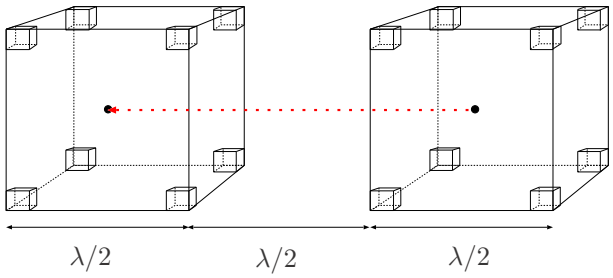

Fig. 4. The test setup used in the numerical experiment

the large (side length $\lambda/2$) cube in 12 separate interpolation steps ($\lambda/8192 \to \lambda/4096 \to \ldots \to \lambda/4 \to \lambda/2$).

Then the out-to-in -translation presented in Section III was performed, followed by the 12-step disaggregation process, and finally the field in the target points (8 cubes with 6^3 points in each) was evaluated and stored in result vector $\tilde{\mathbf{f}}$. It should be noted that in this particular test we only compare the imaginary part of the translated field, see Eq. (1), to the accurate one, as was explained in Section IV. The obtained results, i.e. the relative error defined by formula

$$\frac{\left\| \mathrm{Im}\left(\tilde{\mathbf{f}}\right) - \mathrm{Im}\left(\mathbf{f}\right) \right\|_2}{\left\| \mathrm{Im}\left(\mathbf{f}\right) \right\|_2}, \tag{80}$$

where vector $\mathbf{f}$ contains the directly computed values, are presented in Fig. 5 as function of the chosen accuracy parameter `acc`.

One can clearly observe that the described process works as anticipated, and that it also allows full numerical error control for the translation of the propagating part.

Next the evaluation of whole Eq. (1), employing the processes from Sections III, IV, V and VI, was examined in the same test case. In Fig. 6 the relative error

$$\frac{\left\| \tilde{\mathbf{f}} - \mathbf{f} \right\|_2}{\left\| \mathbf{f} \right\|_2}, \tag{81}$$

is depicted, and in Tables I and II the observed relative speedups compared to the original version by Bogaert et al., see Eq. (3.25) in [11], are shown for the various combinations of accuracy and levels where the translation takes place. The computations for the results shown in the tables were performed in a PC equipped with Intel® E4-1230 v2 processor.

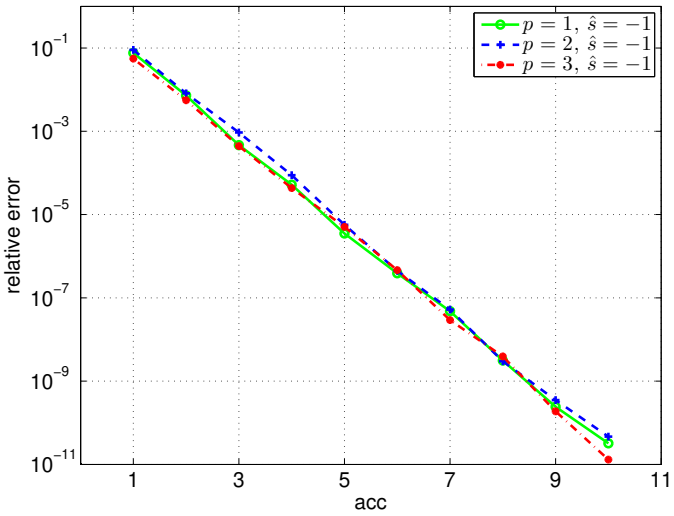

Fig. 5. Demonstration that the algorithms shown in Section III allow full numerical accuracy control for the translation of the imaginary part of the field, see Eq. (1). Results for the cases $\hat{s} = +1$, which are similar, are omitted here.

The developed code utilizes only one thread in these examples, and the `ffts` were computed with Intel® MKL. The variation in the results respect to chosen accuracy and level is due to the sensitivity of the utilized `fft`-library to the length of the processed vectors, see Eq. (60) and (77). No attempt to optimize parameter $\tilde{N}$ in order to improve the CPU-time was done in the results shown in Tables I and II.

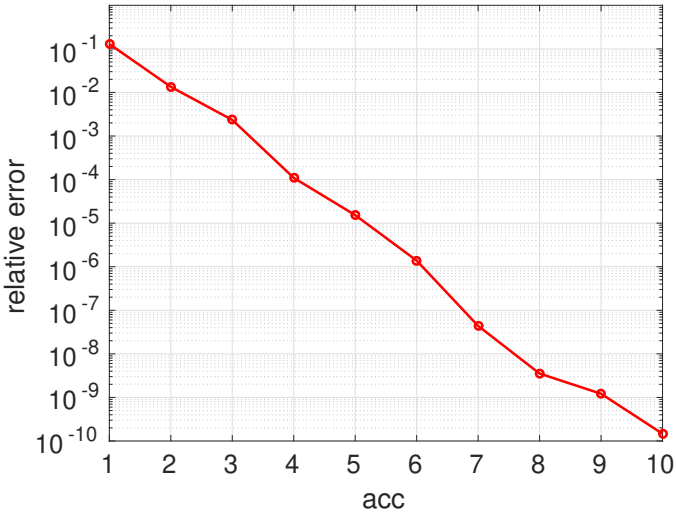

Fig. 6. Relative error of the computed field versus the chosen accuracy.

VIII. Conclusions

In this article some improvements to the broadband TPE-MLFMA based on the use of a spectral translator in lower levels were suggested. A fast algorithm for computing the plane wave samples from multipole series coefficients was presented including the corresponding reverse version. These improvements were derived in detail, and the efficiency of

TABLE I
CONVERSION OF MULTIPOLE SERIES COEFFICIENTS TO PLANE WAVE SAMPLES. SPEEDUP OBTAINED WITH THE NEW ALGORITHM COMPARED TO THE ONE BY BOGAERT ET AL.

	level							
acc	-6	-5	-4	-3	-2	-1	0	1
2	6.0	6.0	5.9	5.9	5.7	7.9	8.6	6.0
3	8.6	8.6	8.5	8.6	8.6	8.3	9.1	8.8
4	12.0	11.8	11.9	11.9	19.4	18.3	12.0	17.1
5	14.1	14.2	14.3	14.3	14.0	25.7	21.4	22.1
6	25.8	25.7	25.7	25.7	25.8	25.2	18.0	31.1

TABLE II
CONVERSION OF PLANE WAVE SAMPLES TO MULTIPOLE SERIES COEFFICIENTS. SPEEDUP OBTAINED WITH THE NEW ALGORITHM COMPARED TO THE ONE BY BOGAERT ET AL.

	level							
acc	-6	-5	-4	-3	-2	-1	0	1
2	4.3	3.8	4.3	3.9	3.6	5.7	6.0	3.9
3	6.0	6.0	6.0	6.0	6.0	5.8	6.0	6.1
4	11.2	11.2	11.2	11.2	20.3	18.1	10.7	15.3
5	13.5	13.6	13.5	13.5	13.5	26.8	21.6	21.0
6	26.0	25.6	25.8	25.7	25.9	25.6	16.1	31.3

was demonstrated with simple examples. These significantly improved conversion algorithms are essential building blocks for developing an efficient and at the same time numerically error controllable MLFMA engine suitable for medium size problems that can be solved in workstation type computers. We have observed that in case of surface integral equation formulations with less than 1 million elements at least half of the CPU-time required for one matrix-vector -product is actually still spent on the conversion process, even with the presented improved formulations.

APPENDIX I

The Fourier series required in Section III for the functions involving characteristic functions of type

$$\chi_{[\alpha,\beta]}(\phi) = \begin{cases} 1, & \phi \in [\alpha,\beta] \\ 0, & \text{otherwise} \end{cases} \tag{82}$$

are as follows:

$$\chi_{[0,\pi]}(\varphi) = \sum_{n=-\infty}^{\infty} a_n^+ \, e^{in\varphi}, \tag{83}$$

$$\chi_{[\pi,2\pi]}(\varphi) = \sum_{n=-\infty}^{\infty} a_n^- \, e^{in\varphi}, \tag{84}$$

$$\tilde{\chi}(\varphi) = \sum_{n=-\infty}^{\infty} i^n a_n^+ \, e^{in\varphi}, \tag{85}$$

$$\chi_{[\frac{\pi}{2},\frac{3\pi}{2}]}(\varphi) = \sum_{n=-\infty}^{\infty} i^n a_n^- \, e^{in\varphi}, \tag{86}$$

$$|\sin\theta| \, \chi_{[\pi,2\pi]}(\theta) = \sum_{m=-\infty}^{\infty} b_m^+ \, e^{im\theta}, \tag{87}$$

$$|\sin\theta| \, \chi_{[0,\pi]}(\theta) = \sum_{m=-\infty}^{\infty} b_m^- \, e^{im\theta}, \tag{88}$$

$$|\sin\theta| \, \tilde{\chi}(\theta) = \sum_{m=-\infty}^{\infty} c_m^+ \, e^{im\theta}, \tag{89}$$

$$|\sin\theta| \, \chi_{[\frac{\pi}{2},\frac{3\pi}{2}]}(\theta) = \sum_{m=-\infty}^{\infty} c_m^- \, e^{im\theta}, \tag{90}$$

where

$$a_n^{\pm} = \begin{cases} \dfrac{1}{2}, & n = 0, \\ \pm\dfrac{i((-1)^n - 1)}{2\pi n}, & \text{otherwise}, \end{cases} \tag{91}$$

$$b_m^{\pm} = \begin{cases} \pm\dfrac{im}{4}, & |m| = 1, \\ \dfrac{1 + (-1)^m}{2\pi(1 - m^2)}, & \text{otherwise}, \end{cases} \tag{92}$$

$$c_m^{\pm} = \begin{cases} \pm\dfrac{1}{2\pi}, & |m| = 1, \\ \dfrac{1}{\pi(1 - m^2)}, & m \text{ is even}, \\ \pm\dfrac{1 - m(-1)^{\frac{m-1}{2}}}{\pi(1 - m^2)}, & \text{otherwise}. \end{cases} \tag{93}$$

APPENDIX II

Let there be coefficient vector

$$\mathbf{a} = [a_0, \ldots, a_N, a_{-N}, \ldots, a_{-1}]^T. \tag{94}$$

Let us then denote sample vector with

$$\mathbf{s} = [s_0, \ldots, s_{2N}]^T, \tag{95}$$

where the elements of this vector are given by

$$s_m = \sum_{n=-N}^{N} a_n e^{-in\frac{2\pi}{2N+1}m}. \tag{96}$$

Then the sample vector $\mathbf{s}$ can be computed efficiently from coefficient vector $\mathbf{a}$ with formula

$$\mathbf{s} = \texttt{fft}(\mathbf{a}). \tag{97}$$

In the previous formula we employ `fft` which computes the Discrete Fourier Transform (DFT) defined by

$$\mathbf{s}(m) = \sum_{n=0}^{2N} \mathbf{a}(n) e^{-i\frac{2\pi}{2N+1}nm}, \quad m = 0, \ldots, 2N. \tag{98}$$

This definition is compatible with the `fft` implementations available for example in MATLAB, FFTW (http://www.fftw.org/) and Intel® MKL. Further if the elements of Eq. (95) are defined as follows

$$s_m = \sum_{n=-N}^{N} a_n e^{in\frac{2\pi}{2N+1}m}, \quad m = 0, \ldots, 2N, \tag{99}$$

then one can evaluate the sample vector $\mathbf{s}$ efficiently with

$$\mathbf{s} = (2N+1) \; \texttt{ifft}(\mathbf{a}). \tag{100}$$

REFERENCES

[1] R. Coifman, V. Rokhlin, and S. Wandzura, "The fast multipole method for the wave equation: a pedestrian prescription", *IEEE Antennas and Propag. Mag.*, vol. 35, no. 3, pp. 7–12, June 1993.

[2] J. M. Song and W. C. Chew, "Multilevel fast multipole algorithm for solving combined field integral equations of electromagnetic scattering", *Microwave Opt. Tech. Lett.*, vol. 10, no. 1, pp. 14–19, Sept. 1995.

[3] W. C. Chew, H. Y. Chao, T. J. Cui, C.-C. Lu, S. Ohnuki, Y.C. Pan, J. M. Song, S. Velamparambil, and J.S. Zhao, "Fast integral equation solvers in computational electromagnetics of complex structures", *Eng. Anal. Boundary Elements*, vol. 27, pp. 803–823, Sep. 2003.

[4] W. C. Chew, J.-M. Song, E. Michielsen, and J. M. Song (Eds.), "Fast and efficient algorithms in computational electromagnetics", Artech House, Boston, 2001.

[5] M. L. Hastriter, S. Ohnuki, and W. C. Chew, "Error control of the translation operator in 3D MLFMA", *Microwave Opt. Tech. Lett.*, vol. 37, no. 3, pp. 184–188, Mar. 2003.

[6] L. J. Jiang and W. C. Chew, "Low-frequency fast inhomogeneous plane-wave algorithm (LF-FIPWA)", *Microwave Opt. Tech. Lett.*, vol. 40, no. 2, pp. 117–122, Jan. 2004.

[7] E. Darve and P. Havé, "A fast multipole method for Maxwell equations stable at all frequencies", *Phil. Trans. R. Soc. Lond.*, A, vol. 362, no. 1816, pp. 603–628, Mar. 2004.

[8] J. Sarvas, "Performing interpolation and anterpolation entirely by fast Fourier transform in the 3-D multilevel fast multipole algorithm", *SIAM J. Numer. Anal.*, vol. 41, no. 6, pp. 2180–2196, 2003.

[9] S. Järvenpää and P. Ylä-Oijala, "A global interpolator with low sample rate for multilevel fast multipole algorithm", *IEEE Trans. Antennas and Propagat.*, vol. 61, no. 3, pp. 1291–1300, Mar. 2013.

[10] S. Järvenpää and P. Ylä-Oijala, "Multilevel fast multipole algorithm with global and local interpolators", *IEEE Trans. Antennas and Propagat.*, vol. 62, no. 9, pp. 4716–4725, Sep. 2014.

[11] I. Bogaert, D. Pissoort, and F. Olyslager, "A faster aggregation for 3-D fast evanescent wave solvers using rotations', *J. Comput. Phys.*, vol. 227, no. 1, pp. 557–573, Nov. 2007.

[12] I. Bogaert, "Broadband multilevel fast multipole methods", Doctoral dissertation, ISBN 978-90-8578-206-3, 2008.

[13] H. Wallén and J. Sarvas, "Translation procedures for broadband MLFMA", *Progr. Electromagn. Res.*, vol. PIER 55, pp. 47–78, 2005.

[14] T. Dufva and J. Sarvas, "Broadband MLFMA with plane wave expansions and optimal memory demand", *IEEE Trans. Antennas and Propagat.*, vol. 57, no. 3, pp. 742–753, Mar. 2009.

[15] N. Yarvin and V. Rokhlin, "Generalized Gaussian quadratures and singular value decompositions of integral operators", *SIAM J. Sci. Comput.*, vol. 20, no. 2, pp. 699–718, 1998.

[16] F. W. J. Olver, A. B. Olde Daalhuis, D. W. Lozier, B. I. Schneider, R. F. Boisvert, C. W. Clark, B. R. Miller and B. V. Saunders, Eds., *NIST Digital Library of Mathematical Functions*, http://dlmf.nist.gov/, Release 1.0.16 of 2017-09-18.

[17] D. Colton and R. Kress, "Inverse acoustic and electromagnetic scattering theory", Applied Mathematical Sciences 93, Springer-Verlag, 1992.

[18] E. P. Wigner, "Group theory and its application to the quantum quantum mechanics of atomic spectra", Academic Press, New York, 1959.

Seppo Järvenpää received the M.Sc. degree in 1992 and the Ph.D. degree in 2001, both in applied mathematics in the University of Helsinki, Finland. Currently he is working as a researcher in Department of Electronics and Nanoengineering in Aalto University, Finland. His field of interest includes numerical techniques in computational electromagnetics based on the integral equation and finite element methods.

Henrik Wallén received the M.Sc. (Tech.) and D.Sc. (Tech.) degrees in Electrical Engineering in 2000 and 2006, respectively, from the Helsinki University of Technology, Finland. He currently works as University Teacher at the Aalto University School of Electrical Engineering, Finland. He also serves as Secretary of the Finnish National Committee of URSI since 2009. His research interests include electromagnetic theory, modeling of complex materials, and computational electromagnetics.